https://doi.org/10.5194/egusphere-2026-1186
Preprint. Discussion started: 9 July 2026

The NASA Microwave Barometric Radar and Sounder (MBARS) airborne instrument and initial flight results

Matthew L. Walker McLinden[1], Bing Lin[2], Nikki C. Privé[1,3], Gerald M. Heymsfield[1,4], Lihua Li[1], Steven Harrah[2], Peter Pantina[1,5], Kevin Horgan[1], and Skylar Hoffert[1]

[1]National Aeronautics and Space Administration (NASA) Goddard Space Flight Center (GSFC), Greenbelt, Maryland 20771, United States of America (USA)
[2]NASA/Langley Research Center (LaRC), Hampton, VA 23681, USA
[3]Goddard Earth Sciences Technology and Research (GESTAR) II, Morgan State University, Baltimore, MD 21251, USA
[4]Earth System Science Interdisciplinary Center (ESSIC), University of Maryland College Park, College Park, MD 20771, USA
[5]Science and Technology Corporation (STC), Hampton, VA 23666, USA

Correspondence: Matthew L. Walker McLinden (matthew.l.mclinden@nasa.gov)

Abstract. The Microwave Barometric Radar and Sounder (MBARS) is a new airborne instrument developed to demonstrate the remote sensing capability of atmospheric sea level pressure (SLP) using a combination of a differential absorption radar (DAR) and a microwave radiometer. The MBARS radar is a near-nadir pointing DAR that operates on the upper side of the V-band oxygen absorption feature, with channels around 65.5, 67.75, and 70 GHz. MBARS recently flew a series of test flights and a science flight on the NASA high-altitude ER-2 aircraft. This paper describes the scientific motivation for the development of MBARS as well as the system hardware, aircraft integration, recent flight activities, and retrieval results. Data from recent flights are presented, showing successful SLP retrievals consistent with science requirements and demonstrating potential for spaceborne applications.

1 Introduction

Modern numerical weather prediction (NWP) models are critically dependent on globally observed meteorological data for their daily operations. These data are an essential part of NWP model initialization, assimilation, improvement, and validation. Some meteorological fields such as temperature and humidity are generally well sampled by both in-situ and remote techniques from surface, suborbital and orbital platforms. Others, such as atmospheric winds, are much less well sampled and are largely indirectly observed through balance with temperature observations. Up until now, sea surface air pressure has only been measured by in situ instruments from ships, buoys, and ocean platforms. There is no operational remote sensing method available for this crucial atmospheric state variable. The spatial distribution of these in-situ instruments is far from uniform, with most observations located near coastlines or along ship tracks. More than 70% of the global ocean is greater than 150 km away from nearest in-situ surface pressure observations, with 25% even more than 500 km away (Privé et al., 2023). Some drifting buoys do not report surface pressures and funding for the drifting buoys is limited (Centurioni et al., 2017). Furthermore, ship-based pressure observations are subject to large errors depending on the type of vessel and the reporting method (Ingleby, 2010).

https://doi.org/10.5194/egusphere-2026-1186
Preprint. Discussion started: 9 July 2026

Surface air pressure is determined by the column total mass of the atmosphere (i.e., dry air plus moisture) and the Earth's gravity acceleration, and can have sharp gradients and subtle features. These pressure and pressure gradient fields are the primary driving force for atmospheric motions that transport mass, moisture and momentum (Holton and Hakim, 2013). NWP models are critically dependent on accurate analyses of the pressure field. Surface pressure observations, mainly over land and some from marine platforms, provide important information about three-dimensional (3D) atmospheric structures and impact on all other model variables including winds throughout the atmospheric volume in assimilation systems (Mass and Madaus, 2014). Studies found that without thousands of surface meteorological stations the 5-to-10-day weather forecasts relied upon daily by the public and commerce would be considerably compromised (Radnóti et al., 2012; Ingleby and Isaksen, 2018). Previous studies have demonstrated that proper knowledge of surface-level pressure can substantially improve hurricane forecasts (Barker et al., 2003, 2004; Xiao et al., 2000, 2009; Min et al., 2015a, b). Recent observing system simulation experiment (OSSE) studies (Privé et al., 2023, 2024) show that NWP models would adjust their modeled pressure fields with satellite-based pressure retrievals as expected and would improve other critical forecasted thermodynamic and dynamic variables such as temperature, humidity, and wind, particularly within the planetary boundary layer (PBL).

Filling the global sea level pressure (SLP) observation gap will provide weather forecast improvements. Recent studies in remote sensing technologies of Differential Absorption Radar (DAR) provide a great potential to fill this SLP observation gap (Lin and Hu, 2005; Lawrence et al., 2011, 2012; Millán et al., 2016; Privé et al., 2023, 2024; Lin et al., 2021, 2023; Battaglia et al., 2024; Lin et al., 2024). Space and airborne remote sensing systems can provide the needed dynamic observations to advance NWP predictions in global and regional scales and for special events such as hurricanes and other severe meteorological systems.

DAR systems for SLP observations are designed to operate at atmospheric oxygen (O_2) absorption bands for column O_2 mass amount measurements. The DAR frequencies (or channels) are chosen to be spectrally close such that environmental impacts such as atmospheric attenuation other than O_2 and sea surface reflection are similar but the difference in O_2 absorption is substantial. Thus, when DAR power returns from the sea surface, the ratios of the channels are measured, and the effects of environmental attenuation and surface reflection are significantly reduced. The differential loss due to atmospheric O_2 is dominant and can be obtained by the ratios of the DAR signals, which leads to the retrieval of column O_2 mass amount. Since oxygen is well mixed in the atmosphere, the column dry air mass can be obtained from the measured O_2 amounts. Additionally, the atmospheric moisture amount is mainly determined by column water vapor with some contributions from cloud water and rainwater in non- or light-rain weather conditions (rain rate < 1 mm hr^{-1}). These moisture values have been well observed by passive microwave, visible, and infrared remote sensing techniques for decades over oceans. Therefore, SLP can be obtained from a combination of the DAR retrievals of dry air mass and the column water, dominantly by water vapor.

The key requirement for the DAR instrumentation is the precision of the SLP retrieval. The standard errors in in-situ buoy and ship observations are generally around 0.9 hPa and between 1.5 hPa and 3 hPa, respectively (Ingleby, 2010; Kent and Berry, 2005). These in-situ SLP measurements have positive impacts on NWP models though data amount is limited (Ingleby and Isaksen, 2018). Recent OSSE studies (Privé et al., 2023, 2024) also demonstrated the positive impact of high precision (within 2 hPa) SLP retrievals from a notional spaceborne DAR on numerical weather prediction. Thus, a precision similar to

https://doi.org/10.5194/egusphere-2026-1186
Preprint. Discussion started: 9 July 2026

in-situ measurements of 2 hPa of SLP retrievals from DAR barometry is required. Since surface air pressure is about 1000 hPa, a 2 hPa standard error would be equivalent to about 0.2% precision. Though challenging, all system design, instrument development and data processing aim at this target. Because of the high precision requirement of SLP retrievals, residual spectral differences from environmental agents such as water vapor, cloud water, rain, and sea surface reflection in the ratio of the power returns of the paired frequency channels would still influence SLP retrieval if only a single spectral pair were used. Thus, a third frequency channel equally spaced spectrally but having weaker O_2 absorption is added. Because of the quasi-linear characteristics of the non-O_2 environmental agents in a narrow spectral width, this third channel is used to mitigate their impacts on the SLP retrieval (Lin et al., 2024).

Based on this concept, NASA Goddard Space Flight Center (GSFC) and NASA Langley Research Center (LaRC) recently developed an airborne sea surface barometry remote sensing instrument named the Microwave Barometric Radar and Sounder (MBARS) to demonstrate atmospheric pressure retrievals for future orbital and suborbital applications. The instrument has been designed with a stable high-precision V-band (65.5 GHz to 70 GHz) DAR combined with a passive microwave radiometer. The passive radiometer within a MBARS system is designed to measure atmospheric temperature profiles. It will support general atmospheric thermal observations and enhance the DAR retrieval capability for vertical pressure profiling, which is beyond the scope of this paper.

The DAR subsystem of MBARS has been built and flown on the NASA high-altitude Earth-Research-2 (ER-2) aircraft. An engineering test flight campaign based out of NASA Armstrong Flight Research Center (AFRC) was conducted during the summer of 2024. MBARS also joined the fall 2024 airborne science campaign of the West-coast & Heartland Hyperspectral Microwave Sensor Intensive Experiment (WH^2yMSIE), also based out of AFRC. One dedicated flight was made during WH^2yMSIE to fly over a sea surface pressure gradient to demonstrate the retrieval. This article reports the approach of MBARS for SLP observation, system design of the radar, hardware development, flight experiments and their results, and the direction of future efforts. Details in general DAR concepts, theoretical bases, retrieval algorithms, and scientific applications can be found in previous publications (Lin and Hu, 2005; Lawrence et al., 2011, 2012; Min et al., 2015a, b; Privé et al., 2023, 2024; Lin et al., 2023, 2024; Battaglia et al., 2024).

Section 2 introduces the basic science requirements for SLP retrievals, and lays out the approach of DAR pressure retrievals. Environmental impacts including sea surface reflection impacts on DAR measurements and retrievals are discussed. Section 3 discusses the DAR instrument design, system considerations, and basic performance of the sensor. Flight campaign test results are presented in Sect. 4. The summaries of current work and future effort directions are provided in Sect. 5.

2 Measurement concept

The theoretical basis of SLP retrieval using DAR system is that environmental conditions, especially atmospheric O_2, have significant impacts on radar signals. Previous work (Lin and Hu, 2005; Lawrence et al., 2011, 2012; Millán et al., 2016; Lin et al., 2024) provided detailed studies about the theory. This paper focuses on the DAR concept that leads to MBARS system design and hardware development. The basic relation between the radar signals and environments, as demonstrated in previous

https://doi.org/10.5194/egusphere-2026-1186
Preprint. Discussion started: 9 July 2026

work, can be approximately expressed as

$$P_r(f) = \frac{\sigma^0(f)}{(4\pi R)^2} P_t(f) A(f) T^2(f) \tag{1}$$

where $P_t(f)$ and $P_r(f)$ are the radar transmitted and received signal powers respectively at frequency f. $A(f)$ is the two-way system gain constant, while $\sigma^0(f)$ is the wavelength-dependent sea surface normalized radar cross section (NRCS) and R is the range from the radar to the surface. $T(f)$ is the one-way atmospheric transmittance at the radar frequency, and will be discussed in more detail below.

Many geophysical variables such as sea surface wind, sea surface water temperature, DAR pointing, incidence, and reflection angles, and sea surface water salinity play important roles in determining the reflectance and/or the NRCS of sea surface. The variations of sea surface NRCS with these variables have been studied for long time. These studies provide theoretical and observational basis of sea surface microwave reflection and their results are widely used in existing mono-static or bi-static Earth-observing radar systems such as those at L, C, X, Ka, Ku, and W bands (Donelan and Pierson, 1987; Masuko et al., 1986; Lin et al., 1999; Stiles and Yueh, 2002; Li et al., 2005; Contreras and Plant, 2006; Tanelli et al., 2008; Foti et al., 2015; Karaev et al., 2015; Hossan and Jones, 2021). Moreover, well measured NRCS values can be used in microwave sensor calibrations (Li et al., 2005). However, it is only recently that sea surface reflection at the O_2 absorption wavelengths of interest (i.e., V-band) has been thoroughly studied (Lin et al., 2023). Key conclusions from the study include: 1) NRCS varies approximately linearly (in dB) with frequency at the considered narrow spectral range under the weather conditions studied; and 2) NRCS values drop quickly with increasing incidence angle. The NRCS at 15^o incidence angle could be reduced by as much as 10 dB or more compared to nadir viewing case, which is one of the crucial factors in system design for a scanning instrument.

$T(f)$ can be expanded as

$$T(f) = \exp\left(-\left(\tau_O(f) + \tau_V(f) + \tau_c(f) + \tau_L(f) + \tau_r(f)\right)/\cos\phi\right), \tag{2}$$

where ϕ is the radar viewing angle relative to nadir and τ_m represents the absorption optical depth (AOD) of atmospheric agent m (m = O_2, vapor, dry air continuum, cloud liquid water, and rainwater or O, V, c, L, and r for short, respectively) at frequency f. Here, non-rain or light rain (rain rate less than 1 mm hr^{-1}) weather conditions are considered. MBARS retrievals from these weather conditions would provide significant weather forecast impacts (Privé et al., 2024). For moderate to heavy rain cases, precipitation-sized large hydrometeors and their related large column total water contents could increase atmospheric absorption and scattering considerably (Lin and Rossow, 1997) and reduce the DAR returns beyond what would be required to retrieve SLP. Thus, these cases are not considered at this time.

A ratio, γ of two spectrally close returns would be:

$$\gamma(f_1, f_2) = \frac{C_2 P_r(f_1)}{C_1 P_r(f_2)} = \frac{C_2 P_t(f_1) A(f_1) \sigma^0(f_1) T^2(f_1)}{C_1 P_t(f_2) A(f_2) \sigma^0(f_2) T^2(f_2)} = \frac{\sigma^0(f_1) T^2(f_1)}{\sigma^0(f_2) T^2(f_2)} \tag{3}$$

where C_1 and C_2 are calibration and normalization coefficients for radar power, antenna, system gain, etc., at frequency f_1 and f_2 respectively. This equation indicates that the calibrated measured power returns of the DAR, or the $\sigma^0 T^2$ in this equation,

https://doi.org/10.5194/egusphere-2026-1186
Preprint. Discussion started: 9 July 2026

can be considered as a measure of the attenuated radar cross section (ARCS, σ_a) that contains critical information about atmospheric absorption. Taking the logarithm of Eq. 3 and reorganizing its order leads to

$$\Delta_{1,2}\tau_O + \Delta_{1,2}\tau_V + \Delta_{1,2}\tau_c + \Delta_{1,2}\tau_L + \Delta_{1,2}\tau_r + \frac{\ln\left(\sigma^0(f_1)/\sigma^0(f_2)\right)}{2}\cos\phi = -\frac{\ln(\gamma(f_1,f_2))}{2}\cos\phi = -\frac{\ln(\sigma_a(f_1)/\sigma_a(f_2))}{2}\cos\phi \quad (4)$$

where $\Delta_{1,2}\tau_m$ represents the difference in AOD (or DAOD) between frequencies 1 and 2 for the agent m. As mentioned in the introduction, the DAOD values except $\Delta\tau_O$ would be small because of the spectral narrowness of f_1 and f_2. Considering the high precision (0.1% to 0.2%) requirement of SLP retrievals, these small DAOD values may still have some impacts on the value in the left side of Eq. 4, which is hoped to be only for O_2. To further mitigate these environmental impacts a third frequency with an equal spectral space as the other two but having weaker O_2 absorption is considered. In this case, the grand ratio, G, of the two ratios of frequency pairs becomes

$$G = \frac{\gamma(f_1,f_2)}{\gamma(f_2,f_3)} = \frac{\sigma^0(f_1)T^2(f_1)\sigma^0(f_3)T^2(f_3)}{\left(\sigma^0(f_2)\right)^2 T^4(f_2)} = \frac{\sigma_a(f_1)\sigma_a(f_3)}{(\sigma_a(f_2))^2} \quad (5)$$

which, similar to Eq. 3 gives

$$\Delta_{1,2}\tau_O - \Delta_{2,3}\tau_O + \Delta_{1,2}\tau_V - \Delta_{2,3}\tau_V + \Delta_{1,2}\tau_c - \Delta_{2,3}\tau_c + \Delta_{1,2}\tau_L - \Delta_{2,3}\tau_L + \Delta_{1,2}\tau_r - \Delta_{2,3}\tau_r = -\frac{\ln(G) - \ln\left(\left(\sigma_1^0\sigma_3^0\right)/\left(\sigma_2^0\right)^2\right)}{2}\cos\phi = \Delta\tau_{3C}. \quad (6)$$

Because of the even-spaced spectra of f_1, f_2, and f_3, and near-linear impacts with frequency of these agents, all terms including sea surface RCS, except $\Delta\tau_O$ are cancelled to a negligible level as shown by Lin et al. (2024). That is,

$$\Delta\tau_{O3C} = \tau_{O1} + \tau_{O3} - 2\tau_{O2} = -\frac{\ln(G)}{2}\cos\phi, \quad (7)$$

or,

$$G_{\mathrm{dB}} = \sigma_{a1\mathrm{dB}} + \sigma_{a3\mathrm{dB}} - 2\sigma_{a2\mathrm{dB}} = -\frac{20\Delta\tau_{O3C}\log_{10}(e)}{\cos\phi} \quad (8)$$

where $\Delta\tau_{O3C}$ is the O_2 DAOD of the three frequencies, while G_{dB} is a common form of G in decibels (hereafter a variable with subscript dB indicates decibels). The oxygen amount can be retrieved from the DAR DAOD measurements due to its direct relation with O_2 AOD and DAOD, as showed previously (Lin and Hu, 2005; Lawrence et al., 2011, 2012; Millán et al., 2016; Lin et al., 2024). Hereafter, this technique of O_2 estimation is called the 3-channel approach. Thus, the partial column dry air pressure for DAR path length is retrieved due to the well mixed O_2 within dry atmosphere (Battaglia et al., 2024; Lin et al., 2024). While the set of frequencies used for MBARS have equal spacing, a similar result can be derived for uneven frequency spacing.

The retrieval of partial-column dry air pressure, P_{dp}, using DAR systems is based on the direct comparison among the O_2 DAOD measurement $\Delta\tau_{O3C\_\mathrm{measured}}$, modeled O_2 DAOD value $\Delta\tau_{O3C\_\mathrm{modeled}}$ and modeled partial column dry air pressure,

https://doi.org/10.5194/egusphere-2026-1186
Preprint. Discussion started: 9 July 2026

P_{dp_modeled}. The latter two are obtained from meteorological profiles with temperature and humidity (T/q) observations or those of NWP models. That is:

$$P_{dp} = P_{dp\_\mathrm{modeled}} \frac{\Delta\tau_{O3C\_\mathrm{measured}}}{\Delta\tau_{O3C\_\mathrm{modeled}}}. \tag{9}$$

SLP, then, is estimated from a combination of dry and moist air pressures:

$$SLP = P_{dp} + P_Z + P_{wp} \tag{10}$$

where P_Z is the pressure at the instrument flight altitude as measured by onboard in-situ sensors. For orbital sensors, $P_Z = 0$. P_{wp} is the partial pressure introduced by atmospheric water along the path length which can be well observed using passive microwave techniques. Equations 9 and 10 are the basic formulas that are used in the SLP retrievals.

The relative SLP error of the DAR retrieval is dominantly decided by the partial column dry air pressure estimates or the measured G of the DAR 3-channel approach. That is, from Eqs. 8 to 10 and for the simplified nadir viewing DAR, the G_{dB} standard error $\mathrm{SE}\{G_{\mathrm{dB}}\}$ would be $20\,\mathrm{SE}\{\Delta\tau_{O3C}\}\log_{10}(e)$ or $8.686\,\mathrm{SE}\{\Delta\tau_{O3C}\}$. The standard error per hPa precision can be estimated as:

$$\mathrm{SE}\{G_{\mathrm{dB}}\} = 8.686\left(\frac{\mathrm{SE}\{\Delta\tau_{O3C}\}}{\Delta\tau_{O3C}}\right)\Delta\tau_{O3C} = 0.020\ (\mathrm{dB\ hPa^{-1}}). \tag{11}$$

Since the value $\Delta\tau_{O3C}$ is about 2.3 (Lin et al., 2024), the standard error of G_{dB} measurements is required to be within 0.04 dB for the SLP retrieval requirement of 2 hPa (approximately 0.2%) given the choice of channels used for MBARS.

The natural phase interactions associated with a radar return from a uniformly distributed surface target cause the received power to fall in an exponential distribution. As the power from many radar returns are averaged the distribution becomes normal with a standard deviation of the estimated received signal power $\hat{P}_r$ equal to the ratio of the total power including noise N and the square root of the number of independent samples M_i (Fukao et al., 2014),

$$\mathrm{SD}\{\hat{P}_r\} = \frac{P_r + N}{\sqrt{M_I}}. \tag{12}$$

Therefore, to minimize the standard deviation of the measured signal power the number of independent samples must be maximized while maintaining a sufficiently high signal-to-noise ratio (SNR).

Based on the first-order error propagation theory, the fractional standard deviation of the measured grand ratio $\hat{G}$ is approximately

$$\frac{\mathrm{SD}[\hat{G}]}{G} = \left(\left(\frac{\mathrm{SD}[\hat{P}_{r1}]}{P_{r1}}\right)^2 + 4\left(\frac{\mathrm{SD}[\hat{P}_{r2}]}{P_{r2}}\right)^2 + \left(\frac{\mathrm{SD}[\hat{P}_{r3}]}{P_{r3}}\right)^2\right)^{\frac{1}{2}}. \tag{13}$$

In practice, the signal-to-noise ratio for channels 2 and 3 will be much higher than channel 1 due to the significant atmospheric attenuation at 65.5 GHz. Substituting Eq. 12 into Eq. 13 and including only the first-order term of the SNR of channel 1 gives an estimation of the overall fractional standard deviation of the grand ratio as a function of the SNR and number of independent

https://doi.org/10.5194/egusphere-2026-1186
Preprint. Discussion started: 9 July 2026

samples measured at the three frequencies,

$$\frac{\mathrm{SD}[\hat{G}]}{G} \approx \left(\frac{1}{M_{I1}} + \frac{2}{(SNR_1)M_{I1}} + \frac{4}{M_{I2}} + \frac{1}{M_{I3}} \right)^{\frac{1}{2}}. \tag{14}$$

The key then is maximizing the number of independent samples within the spatial resolution, particularly at channel 2, while maintaining a sufficiently positive signal-to-noise ratio. In addition to this, the instrument must maintain stability sufficient to prevent systematic drifts between the channels approaching the 0.04 dB target. The total number of independent samples to achieve 2 hPa SLP precision is on the order of 100,000 samples per channel.

3 Airborne instrument description

MBARS is a V-band (65.5-70 GHz) sensor initially developed to fly on the NASA high-altitude ER-2 aircraft in a wing-mounted “superpod". The radio frequency (RF) transceiver and antenna subsystems are mounted in the unpressurized superpod aft-body where the beam of the two-axis scanning antenna system points through an open window. The aft-body MBARS subsystems are shown in Fig. 1. The power distribution unit (PDU), radar digital unit (RDU), and the intermediate frequency (IF) boxes are mounted on a horizontal rack in the pressurized superpod midbody. The system block diagram is shown in Fig. 2. This section describes the MBARS systems and the instrument’s installation on the ER-2 aircraft.

MBARS interfaces electrically with the ER-2 through the Experimenter’s Interface Panel (EIP). The system receives both 28 V direct current (DC) and three-phase 400 Hz 120 V alternating current (AC) power. The pilot has ultimate control over the radar through two interlock switches. The first interlock switch enables power to the radar system, and the second enables transmit. An additional altitude switch prevents accidental radar transmission on the ground.

Control software within the RDU enables MBARS to run autonomously. Subsystems are powered sequentially with regular autonomous fault checking. The RDU then commands transmit and antenna beam scanning when the radar is in a safe condition and transmit has been enabled by the hardware interlocks. A remote radar operator may modify the radar state with commands issued through a terminal or socket interface. This autonomous operation is optimized to enable MBARS to operate without significant input from the pilot or remote instrument operators.

To meet the measurement performance requirements discussed in Sect. 2, MBARS uses an extended frequency-diversity waveform, a solid-state power amplifier (SSPA), and a 0.3 m lens antenna. A summary of the performance metrics of MBARS is given in Table 1.

The design in some ways exceeds the theoretical requirements for pressure retrievals. This design enables MBARS to be used to test the effects of instrument performance on retrievals to validate the theoretical calculations. As an example, the narrow cross-track scan and pitch control allow testing of the optimal incidence angle of ARCS measurements for SLP retrievals. This flexibility also provides the ability to evaluate the system architecture for future spaceborne applications.

https://doi.org/10.5194/egusphere-2026-1186
Preprint. Discussion started: 9 July 2026

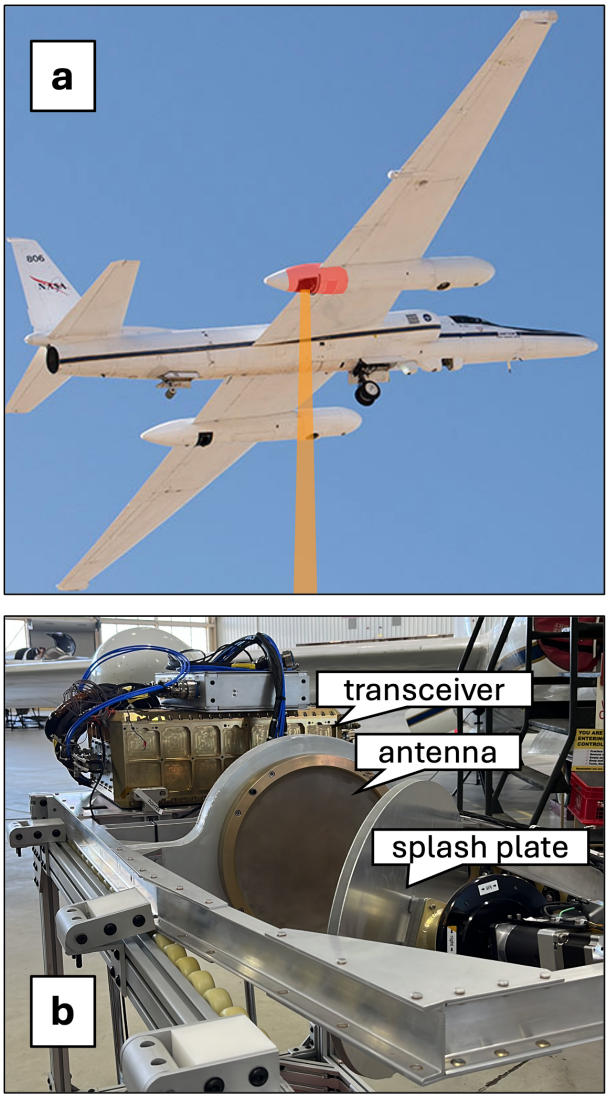

Figure 1. (a) The NASA ER-2 with the location of MBARS in the aft-section of the superpod highlighted in red and the radar beam illustrated in orange. Photograph by Carla Thomas, NASA. (b) The MBARS aft-body subsystems including the hermetic transceiver, lens antenna, and scanning splash plate ready for installation.

https://doi.org/10.5194/egusphere-2026-1186
Preprint. Discussion started: 9 July 2026

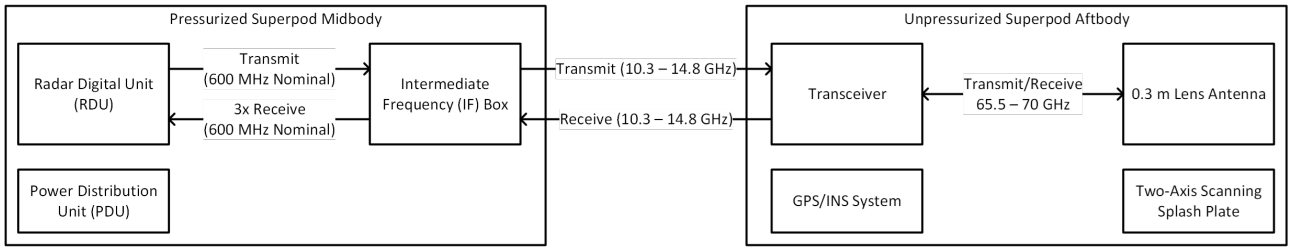

Figure 2. The MBARS block diagram includes subsystems located within the pressurized superpod mid-body of the ER-2 as well as the unpressurized superpod aft-body.

Table 1. MBARS Performance Metrics

Parameter	Instrument performance
Transmit frequency	65.5, 67.75, 70 GHz nominal
Transmitter power	5.9 W at 65.5 GHz 4.5 W at 67.75 GHz 1.6 W at 70 GHz
Receiver noise figure	9 dB
Pulse Repetition Interval (PRI)	420 μs
Pulses per PRI	4x 18 μs pulses near 65.5 GHz 7x 1.8 μs pulses near 67.75 GHz 4x 1.8 μs pulses near 70 GHz 25 μs, 3 MHz chirp near 70 GHz
# of frequency-diversity waveforms	4
Waveform repeat interval	1.68 ms
Antenna diameter/yype	0.3 m lens
Antenna 3 dB beamwidth	1 degree
Beam pointing control	$\pm 15^o$ cross-track $\pm 5^o$ pitch compensation
Total instrument mass	119 kg
Total power (including heaters)	1670 W

3.1 Waveform design and frequency diversity

The frequency-diversity waveform was a driving design consideration of MBARS. The precision to achieve 1-2 hPa pressure retrievals requires a large number of independent samples. Samples may be decorrelated by varying the frequency (as with frequency diversity) or moving the antenna (as with the forward motion of the aircraft). MBARS uses both techniques to increase the number of independent samples.

https://doi.org/10.5194/egusphere-2026-1186
Preprint. Discussion started: 9 July 2026

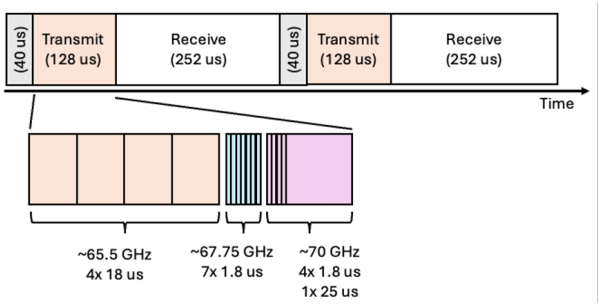

Figure 3. Time-domain illustration of the frequency-diversity waveform. Individual pulses are offset from the nominal channel frequencies within 150 MHz bands. Four long (18 μs) pulses are transmitted near 65.5 GHz, followed by seven shorter (1.8 μs) pulses near 67.75 GHz. Finally, four short pulses and a 25 μs chirp are transmitted near 70 GHz.

During each pulse repetition interval (PRI), MBARS transmits fifteen pulses and one chirp. First, four 18 μs pulses are transmitted near 65.5 GHz but at slightly offset frequencies. The relatively long pulse length and the associated narrow matched-filter bandwidth enables the received ARCS measurements to have a sufficiently positive SNR of approximately 8 dB even with the significant round-trip attenuation of oxygen at this frequency. Seven frequency-separated 1.8 μs pulses are then transmitted near 67.75 GHz followed by four frequency-separated 1.8 μs pulses transmitted near 70 GHz. These narrower pulses still provide sufficient SNR due to the reduced oxygen attenuation at 67.75 and 70 GHz. Finally, a 25 μs chirp with a 3 MHz bandwidth is transmitted near 70 GHz. This chirp is not directly used in atmospheric pressure retrievals but provides a vertical profile of clouds and precipitation. The waveform is illustrated in time domain in Fig. 3.

After transmitting the fifteen pulses and single chirp the radar receives the echoes at all sixteen subchannels simultaneously. The three main frequency channels (near 65.5, 67.75, and 70 GHz) are separated and downconverted using RF electronics and the subchannels are separated using digital filtering and downconversion after sampling by the analog-to-digital converters (ADCs). Assuming the frequency separation of the subchannels is sufficient for full decorrelation, this single PRI provides four independent samples of surface scatter around 65.5 and 70 GHz, and seven independent samples of surface scatter around 67.75 GHz.

The MBARS antenna is 0.3 m in diameter, so neglecting motion of the ocean surface, full decorrelation of repeated radar pulses at a constant frequency will only occur when the radar has moved by a full 0.3 m perpendicularly to the beam. The MBARS antenna moves by approximately 8.4 cm in the along-track direction during a single 420 μs pulse repetition interval (PRI) on the ER-2 with a ground speed of approximately 200 m s^{-1}. As such, upon completion of a PRI the process repeats with all pulses frequency-hopped to new subchannels (the chirp frequency remains constant). The instrument cycles through four complete waveforms (sets of subchannels), repeating every 1.68 ms. During this 1.68 ms the aircraft has moved by approximately 0.34 m, allowing reuse of subchannel frequencies without correlated surface backscatter.

Within the three main frequency channels, frequency-diversity subchannels are separated by at least 4 MHz. Individual pulses and the chirp are amplitude tapered with Hann windows at the waveform generator. The SSPA is then driven to compres-

https://doi.org/10.5194/egusphere-2026-1186
Preprint. Discussion started: 9 July 2026

sion. The result is a pulse amplitude that is a compromise between maximizing transmitted power and obtaining subchannel-subchannel isolation.

3.2 Instrument subsystems

3.2.1 Antenna and scanner

The MBARS antenna aperture is a 0.3 m polystyrene lens. This antenna uses an internal wire-grid polarimetric reflector to share the lens between two orthogonal feeds, one port for the V-band MBARS frequencies and a second feed for W-band near 94 GHz. While not used by MBARS, this second feed provides the possibility of sharing the antenna aperture with a second radar such as the airborne NASA Cloud Radar System (CRS) (Walker McLinden et al., 2021). This antenna is visible in Fig. 1 and is located in the unpressurized aft section of the superpod. The measured gain of the antenna is 44 dB at V-band.

A flat honeycomb splash plate mirror is used to redirect the beam from the lens antenna to near-nadir view angles through an open port in the superpod. This splash plate is connected to a two-axis scanner, allowing 360^o of motion in the cross-track direction and $\pm 5^o$ of motion in the along-track direction. The along-track scanning is used to provide real-time pitch compensation to allow the angle of the beam to be controlled through aircraft pitch variations. The cross-track control allows for beam scanning up to $\pm 15^o$ off-nadir, or for a controlled incidence angle even in the case of aircraft roll variation and wing flex. The scanner is software-controlled by the radar command and data handling (C&DH) computer based on attitude data from an onboard global positioning system (GPS) and inertial navigation system (INS) receiver.

3.2.2 Solid-state transceiver

The solid-state transceiver is located in the unpressurized aft section of the superpod, housed in a hermetic enclosure that maintains air pressure even at the approximately 20 km flight altitude of the ER-2. The transceiver is built with WR-15 waveguide electronics combined with some coaxial components. The simplified radio frequency (RF) block diagram is shown in Fig. 4.

The transceiver is broadband, covering 65.5 to 70 GHz. The system inputs the frequency-diverse waveform at an intermediate frequency (IF) of 10.3-14.8 GHz, and upconverts it to RF. The waveform at RF frequencies is then amplified by two broadband amplifiers followed by the SSPA. The Gallium Nitride (GaN) SSPA is optimized for transmit power at 65.5 GHz, with a saturated power of 5.9 W. The transmitted power decreases at the higher transmit frequencies, with saturated power of 4.5 W at 67.75 GHz and 1.6 W at 70 GHz. The transmitter and waveform generator are tuned such that the SSPA is driven into saturation for all pulses to maximize radar sensitivity.

Duplexing is achieved with a broadband waveguide circulator. Two pin diode switches protect the low-noise amplifier (LNA) from being damaged by excessive RF power during the transmit window. Received signals are amplified by a LNA and a gain stage before being mixed back to 10.3-14.8 GHz. Mixing for both up-conversion and down-conversion is achieved with balanced mixers. A single phase-locked oscillator (PLO) at 13.8 GHz drives a x4 multiplier for each mixer.

https://doi.org/10.5194/egusphere-2026-1186
Preprint. Discussion started: 9 July 2026

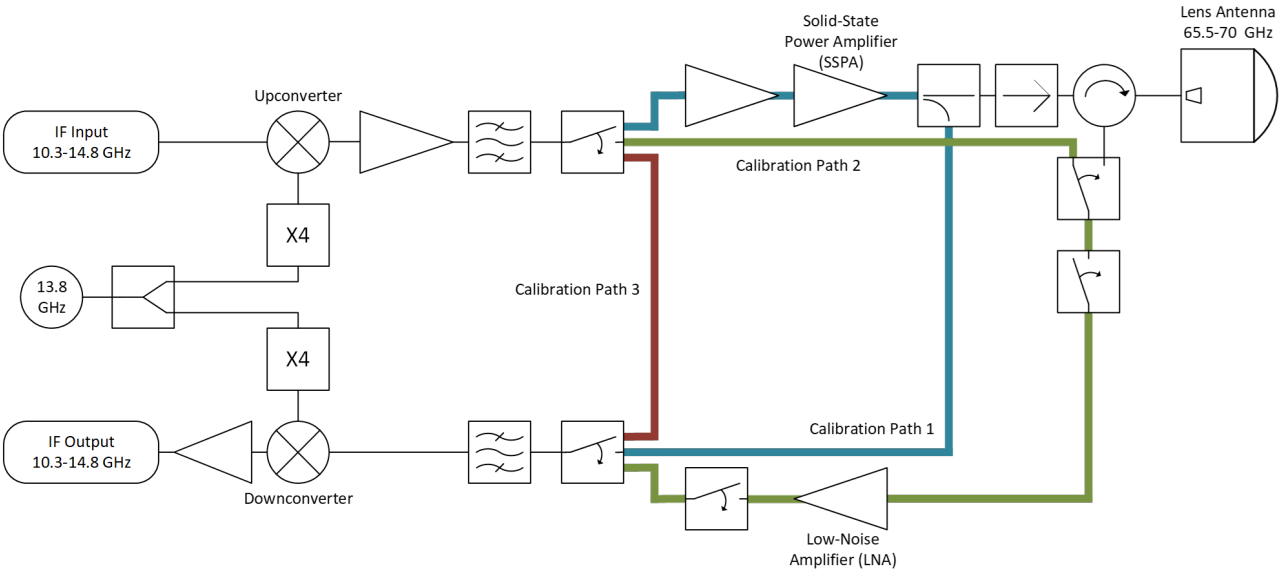

Figure 4. The simplified transceiver RF block diagram showing the three internal calibration paths used to track variations in system gain (discussed in more detail in Sect. 3.3).

Calibration is achieved with a set of three calibration paths controlled by pin-diode switches. These three paths are shown in Fig. 4 and are discussed in more detail in Sect. 3.3. There are additional secondary calibration electronics including an electromechanical “baseball" waveguide switch, a detector diode, and a noise diode. This redundant approach to calibration was selected due to the experimental nature of this instrument, so as to allow comparison of different calibration approaches. In practice, only the primary calibration paths are used due to their superior performance, and the additional calibration electronics are not shown in Fig. 4 for simplicity.

As the precision and calibration requirements are very stringent, particular care was made to maximize the linearity of the receiver. Attenuators set the gain such that the maximum power presented to any active component in the receiver chain is 20 dB below the one-decibel compression point (P1dB). The exceptions to this rule are the receiver amplifiers during transmit as they are disabled by the following calibration-path pin switches.

3.2.3 Radar digital unit

Radar control and coordination occurs through a Linux-based single-board computer (SBC). This computer is networked to four field-programmable gate array (FPGA)-based radar processing modules, a system timing and control unit, and a GPS/INS receiver through a gigabit-speed internal Ethernet network. The SBC also provides a separate Ethernet connection to the aircraft network to enable remote radar operator control and near-real time visualization of radar data. It interfaces with the antenna scanner system through RS-232 and onboard telemetry and relay systems through RS-485. All radar data are recorded onto removable USB-based storage devices connected to the SBC.

https://doi.org/10.5194/egusphere-2026-1186
Preprint. Discussion started: 9 July 2026

Software running on the SBC provides autonomous system control. This software is designed to operate with or without inputs from a radar operator. It powers radar systems and controls the radar beam scanner and transmitter based on instrument telemetry, the status of an aircraft altitude interlock switch, and two control switches operated by the pilot. The instrument state may be modified by a remote operator through socket-based commands.

The MBARS radar-control modules developed by Tomorrow.io provide waveform generation, digital receiving, and switch control. The radar system utilizes a waveform generator module, two digital receiver modules, and a switch-control module. The waveform generator module includes a single digital-to-analog converter (DAC) and each digital receiver module includes two analog-to-digital converter (ADC) and can process eight frequency-diverse subchannels simultaneously.

The waveform generator DAC operates at 2.4 GSPS. The frequency-diversity transmitted waveforms are generated within a 150 MHz bandwidth centered at 600 MHz. A pin diode switch is used to divide each waveform into the three radar channels and routes each channel to a separate up-conversion mixer. The waveform generator sequences through the four independent waveforms, repeating each waveform every four pulse repetition intervals (PRI's).

The radar system's four ADCs also operate at 2.4 GSPS. The IF subsystem down-converts the three radar RF channels simultaneously to be centered at 600 MHz, routing the 65.5 GHz channel and 67.75 GHz channel to one ADC each, and routing the 70 GHz to two ADCs. The digital system digitally down-converts, filters, and decimates each of the sixteen subchannels. The channels are then passed through approximately matched filters (or a pulse compression filter for the chirp).

3.2.4 Intermediate frequency

The intermediate frequency (IF) subsystem upconverts the signal generated by the waveform generator (within a 150 MHz band around 600 MHz) to the three intermediate bands provided to the transceiver subsystem (at 10.3 GHz, 12.55 GHz, and 14.8 GHz respectively). The upconversion to the three IF bands occurs sequentially during the waveform generation as the local oscillator and anti-aliasing filter is switched. While the subchannels are transmitted sequentially, they must be received simultaneously so the received IF signal is split into three IF bands, filtered, and then further downconverted to 600 MHz in parallel.

3.2.5 Flight-level pressure sensors

The MBARS DAR retrieval provides the contribution of dry air below the radar to the atmospheric surface pressure . As such, the air pressure at the flight level must be known independently. MBARS flies with two absolute pressure transducers each with 0.2 hPa precision and stability. These transducers are connected to separate static pressure ports on the ER-2 aircraft and provide the means to track the flight-level pressure.

At flight altitude during test flights these pressure sensors measured a mean flight-level pressure of 56.3 hPa with a standard deviation of 1 hPa. The pressure reported by the two sensors differed by 1.1 hPa with a 0.04 hPa standard deviation. The calibration approach of MBARS is to use vicarious sources so the bias does not impact the retrieval. The low standard deviation provides confidence that these sensors are sufficient to track flight-level pressure changes without driving overall retrieval uncertainty.

https://doi.org/10.5194/egusphere-2026-1186
Preprint. Discussion started: 9 July 2026

3.3 Calibration

Absolute calibration of MBARS to the accuracy required is infeasible using internal calibration methods, even with the three-path calibration strategy (see below). As such, an external calibration is required to provide absolute calibration. MBARS absolute calibration is performed vicariously, using a known sea surface pressure (provided either by one or more buoy measurements or model data from a stable high-pressure system when in situ measurements are not available). In this way MBARS fundamentally tracks pressure changes from a reference rather than providing an absolute measurement during its flight experiments. It is possible that the careful internal calibration and temperature monitoring could make MBARS sufficiently stable to keep the instrument operating at a predetermined condition and maintain absolute calibration between flights, but this has not been attempted.

The MBARS transceiver was developed with redundant internal calibration strategies due to the extreme (<0.02 dB) stability requirements. The primary calibration approach is a three-path loopback in the RF transceiver. Secondary calibration approaches include a single loopback path utilizing an electro-mechanical switch and the combination of a noise diode and detector diodes. Finally, the transceiver was designed to allow for external calibration including a nadir-pointing cold-sky horn antenna and a blackbody absorber load, however these external calibration sources have not been implemented. Only the primary three-path loopback has been used to-date due to its superior stability.

Loopback calibration takes advantage of the fact that the radar equation includes the product of the transmitted power, range weighting function, and the receiver gain. As such, tracking of individual contributors is not required (see Eq. 3). With any loopback calibration the primary metrics of the calibration are stability of the calibration path and the ratio of the power of the transmitted signal through the calibration path to any secondary paths caused by radiated or conducted leakage. The relative phase of any leakage as compared to the desired calibration path cannot be assumed to be stable, so the presence of any leaked power provides a variable error. For a typical atmospheric radar, the calibration path may be 30 dB stronger than any leakage, resulting in a peak calibration offset of approximately $\pm$0.3 dB. MBARS, with its stringent stability requirement has a designed signal-to-leakage ratio better than 53 dB, for a stability better than $\pm$0.02 dB irrespective of potential relative phase changes in the leakage path.

This stringent signal-to-leakage drove the design of the radar calibration paths. The maximum power of the signal through the received calibration path is limited by the linearity of the receiver. Reducing the leakage through the calibration paths requires not only lossy switches (impacting noise figure) but care with managing radiated and conducted emissions. To address these competing interests, the MBARS calibration is split into three paths, each with a more modest dynamic range than a single-path design.

For the first calibration path (labelled as Calibration Path 1 in Fig. 4), a portion of the waveform during transmit is coupled out after the SSPA and is switched into the receiver after the LNA and gain stage. Excluding the first two stages of receiver amplification from this calibration path minimizes the susceptibility of the system to radiated or conducted leakage paths and allows for placement of some pin switches after the LNA, improving the system noise figure. This calibration loop tracks most

https://doi.org/10.5194/egusphere-2026-1186
Preprint. Discussion started: 9 July 2026

system fluctuations in the transmit and receive paths but does not capture gain variations in the LNA or receiver protection switches.

Two additional loopback paths are included to track gain fluctuations in the LNA and receiver protection switches. One or more times per second, the waveform generator produces a second copy of the transmitted waveform during the nominal receive window. This waveform, rather than being sent to the SSPA, is coupled to the input of the LNA (Calibraiton Path 2) with the receiver protection switches blocking the received signal from the antenna. Alternatively (Calibration Path 3), the second waveform is looped back directly to the downconversion receiver mixer bypassing both the SSPA and LNA. The ratio of the measured calibration signal from these two paths provides the mechanism for tracking LNA gain variations. Monitoring these calibration paths while the SSPA is disabled minimizes the presence of leakage signals (improving the ratio of calibration power to leakage). These loopback paths are exercised during the nominal receiving window between transmitted pulses to avoid interrupting the duty cycle of the SSPA, as the resulting thermal drift may cause calibration instability.

4 Airborne flight results

MBARS was deployed to NASA AFRC and installed into the NASA ER-2 aircraft for evaluation of its DAR system performance, SLP observational capability and future space flight potential. An initial test flight campaign was conducted during the summer of 2024 for DAR engineering test. System stability and performance were evaluated. Later in the fall of 2024, the MBARS joined the WH^2yMSIE flight campaign and successfully collected DAR data with significant sea surface air pressure variations. The open ocean off the west coast of California was the primary target for these MBARS flight experiments. This section discusses MBARS performance and SLP retrievals under both uniform sea surface pressure and significant SLP gradient conditions.

Large oceanic areas off the west coast of California generally lack large atmospheric disturbances in the northern hemispheric summer season. During the period of the engineering test flight campaign in the summer of 2024, the sea surfaces targeted were generally quiet, which allowed the assessment of instrument stability and potential retrieval uncertainties. An example was the 17 July 2024 case. This same oceanic area, however, experienced more substantial weather variations during the fall of 2024. Thus, SLP retrievals with MBARS measurements could be evaluated, such as for the case with a significant SLP gradient on 13 November 2024. MBARS flight experiments were conducted for those two days. Figure 5 shows the flight tracks of those two cases. To avoid land contamination and island impact, only MBARS measurements collected at least 10 km away from the coastline and islands were used in data analysis and SLP retrieval.

A hardware issue within the networking subsystem of MBARS resulted in significant data loss (50-75%) during all flights, particularly during the November 2024 case. While since corrected, this issue caused irregular gaps in the recorded backscatter signal of these cases. These gaps in data complicate the analysis and the ability to average beyond 10 seconds, and are the cause of the irregularly spaced datapoints within the retrieval data shown here.

During the flight of 17 July 2024, the ER-2 repeated an extended flight track three times, as indicated in Fig. 5 (a), to evaluate system stability and SLP retrieval uncertainties for a relatively uniform marine environment with SLP variability only about 0.4

https://doi.org/10.5194/egusphere-2026-1186
Preprint. Discussion started: 9 July 2026

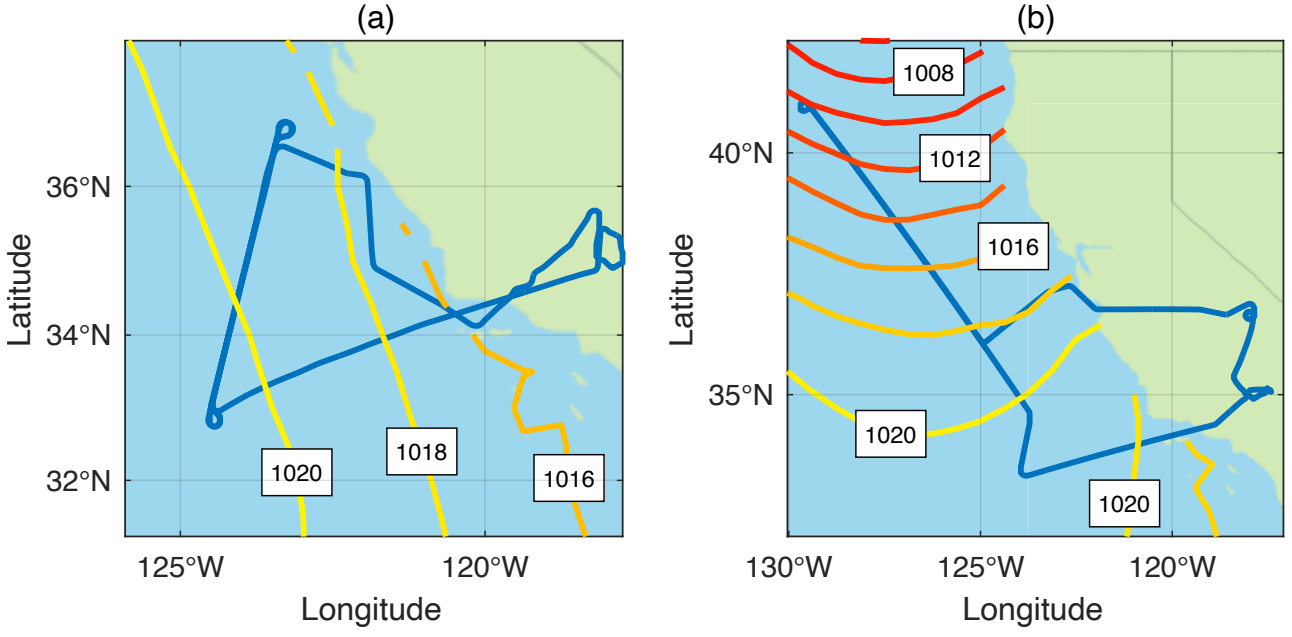

Figure 5. The flight track of MBARS on the ER-2 during the two dates used for radar and algorithm evaluation along with sea level pressures (hPa) from the MERRA-2 reanalysis. (a) 17 July 2024. (b) 13 November 2024. The underlying map is MATLAB Basemap Data - bluegreen, created using Natural Earth.

hPa. The MBARS instrument as a whole was very stable during the entire flight. Calibration subsystem tracked the variations of DAR individual components well. Figure 6 shows the relative precision changes of DAOD with averaging time. Different color points represent different legs of the segment as indicated in the figure and the dashed line is the precision predicted by Eq. 14. The precision improves with longer averaging. The standard deviation drops at a rate slightly slower than predicted for the longer averaging periods, indicating some level of calibration instability or $1/f$ noise. The DAOD values obtained from ARCS measurements of MBARS still reached the required 0.2% precision after 10 s integration for this stable meteorological condition case.

To retrieve SLP with MBARS ARCS measurements, an ancillary data of the Modern-Era Retrospective analysis for Research and Applications, Version 2 (MERRA-2) reanalysis of the Goddard Earth Observing System Model version 5 (GEOS-5) from the NASA Goddard Modeling and Assimilation Office (Gelaro et al., 2017) was used because of lack of observed atmospheric meteorological state information for the flight campaigns. The MERRA-2 dataset provides the basic meteorological profiles for forward calculations of the modeled DAOD values in partial column dry air pressure retrieval (ref., Eq. 7 or Eq. 8). The temperature sounder of MBARS has not been tested at this stage. The MBARS sounder measurements and temperature and humidity observations from other sensors will be used in future retrievals, which would potentially improve MBARS SLP observations. Additionally, there were no buoy or other in-situ data available near the tracks of the MBARS experimental flights. MBARS SLP retrievals were compared to the MERRA-2 data. Analyzing MERRA-2 and buoy data along the west coast

https://doi.org/10.5194/egusphere-2026-1186
Preprint. Discussion started: 9 July 2026

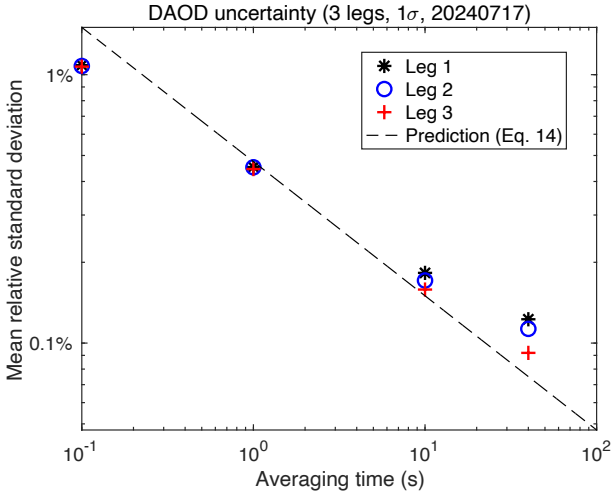

Figure 6. The MBARS system is stable such that averaging of radar samples continues to reduce the standard deviation of the measurement beyond ten seconds (corresponding to approximately 2 km flight distance) to achieve the required 0.2% uncertainty. The standard deviation of the three flight legs are shown individually, along with the predicted standard deviation derived from Eq. 14.

near the flight field domain, a reasonably small standard error (STD) of 0.8 hPa was found, which was consistent with previous studies (e.g., Ingleby, 2010). This indicates that NWP models such as GOES-5 can provide reasonably good SLP results near coast areas where certain buoy and other in-situ observations are available for NWP models as pointed out by previous studies (Whitaker et al., 2004; Dirren et al., 2007). Future scientific field campaigns with sufficient in-situ observations will provide better retrieval validations.

Furthermore, although the V-band O_2 absorption model (Liebe et al., 1993) has been used in passive microwave temperature profiling for decides and even in many DAR simulation studies (e.g., Lin et al. (2024) and references therein), this is the first time that DAR measurements are used in quantitative precise SLP retrieval. Potentially both DAR measured signals and the microwave radiative transfer model could have non-negligible absolute calibration errors for the extremely high accuracy needs when relative errors less than 0.2% are required. Thus, another use of MERRA-2 data in SLP retrieval was for MBARS absolute calibration when observations of in-situ SLP and atmospheric meteorological state profile were not available. In this study, MBARS DAOD measurements were directly compared to the modeled DAOD values for a very small amount of oceanic data at the beginning of individual flights. Small, averaged differences between the two kinds of DAODs for individual flights were found and removed from MBARS measured DAOD values, which was considered as a way to provide the absolute calibration of MBARS measured DAODs. In the future, using actual buoy and in-situ surface SLP observations, along with observed atmospheric meteorological state profiles, advanced absolute calibrations of MBARS measurements and, potentially, the microwave radiative transfer model are expected.

Figure 7 shows the SLP retrieval results of the three legs for 10 s averaged data. There are no clear trends for all three leg retrievals. The standard error for the retrievals of all three legs combined is 1.64 hPa with individual legs varying from 1.48 to

https://doi.org/10.5194/egusphere-2026-1186
Preprint. Discussion started: 9 July 2026

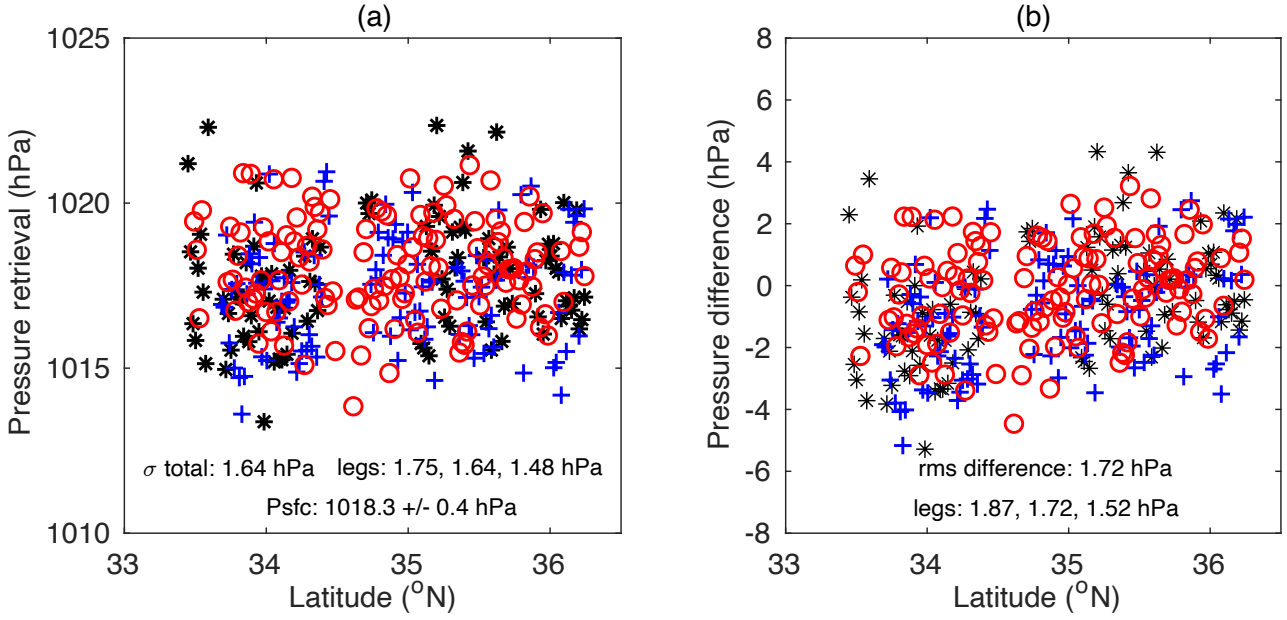

Figure 7. (a) The MBARS pressure retrievals using 10 s averaging over three flight legs (calibrated to MERRA-2 at the start of the first flight leg) in the July 2024 high-pressure system case chosen for having minimal pressure variation. (b) The surface pressure difference between the pressure retrievals and the MERRA-2 reanalysis over the three flight legs showing an RMS difference of less than 1.9 hPa for all three flight legs.

1.75 hPa. The root mean square (RMS) errors are also small, just slightly larger than their corresponding STD values. These results provide a strong confidence in using MBARS for SLP retrieval.

The retrievals of the fall of 2024 case further exhibit the MBARS capability for SLP observations (Fig. 8). For this case, a significant sea surface air pressure variability of about 7 hPa occurred, as shown in Fig. 5b and Fig. 8a. The ER-2 flew over a the pressure gradient field. The MBARS 10 s SLP retrievals (Fig. 8a) were similar to the sea surface pressure values. The STD and RMS errors of these 10 s averaged SLP retrievals are about 2.35 hPa and 2.40 hPa, respectively. As mentioned in Sect. 2, the DAR system design targeted at 20 s averaging to achieve 2 hPa precision for SLP retrievals. Scaling by $1/\sqrt{2}$ to the current data obtained from a half-length of the needed averaging time period would achieve the required precision, illustrating the advanced capability of the airborne MBARS system in SLP observations and providing a great potential of the MBARS measurements to meet science requirements for future applications in improving NWP model forecasts.

5 Conclusions

The MBARS instrument was developed as a stable and precise radar using a solid-state transceiver and frequency diversity that flies on the NASA ER-2 high-altitude aircraft. Engineering test flights and one science flight during the WH^{2}yMSIE field campaign demonstrate a standard deviation of measured DAOD of less than 0.2% with 20 s integration. The retrieved sea-level

https://doi.org/10.5194/egusphere-2026-1186
Preprint. Discussion started: 9 July 2026

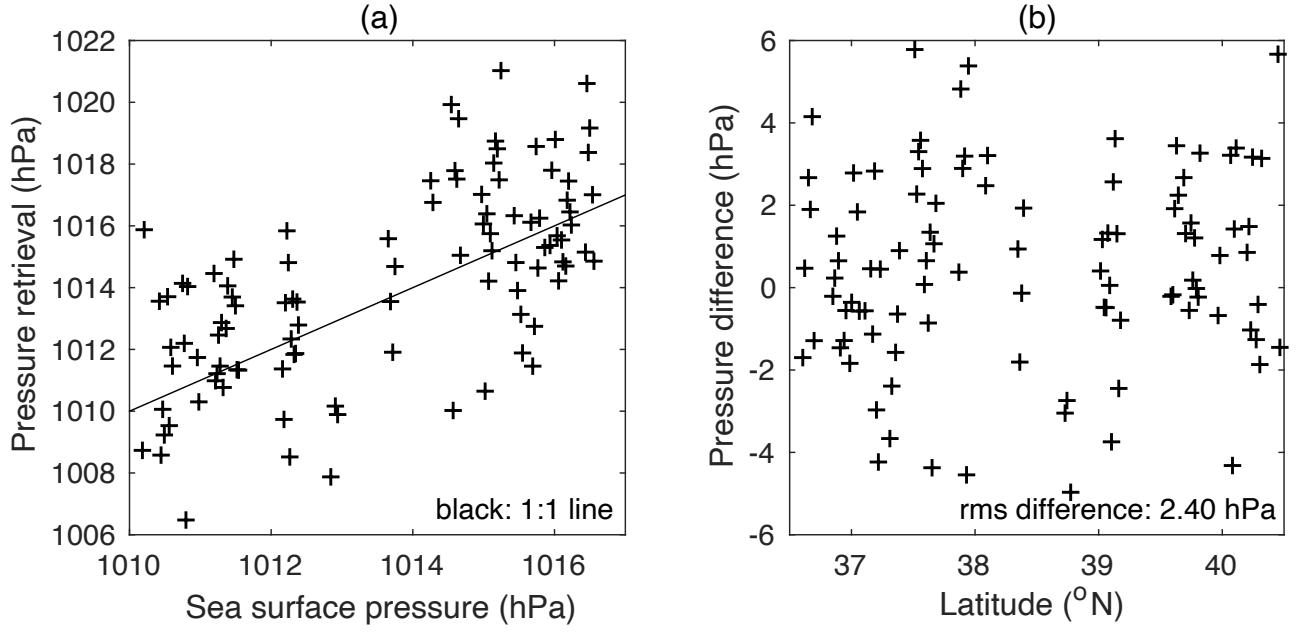

Figure 8. (a) The MBARS pressure retrievals using 10 s averaging over the 7 hPa pressure gradient in the November 2024 case calibrated to MERRA-2 at the start of the first flight leg. (b) The difference between the pressure retrievals and the MERRA-2 reanalysis showing am RMS difference of 2.4 hPa.

pressure using 10 s averaging (rather than 20 s due to data loss and gaps in these initial flights) tracks the MERRA-2 reanalysis model to 1.7 hPa RMS for the first flight and 2.4 hPa RMS for the second. The projected performance with 20 s averaging is within the target performance of 2 hPa precision.

Work is ongoing to integrate MBARS onto NASA's new Boeing 777 airborne science platform and participation in the North American Upstream Feature-Resolving and Tropopause Uncertainty Reconnaissance Experiment (NURTURE) scheduled for early 2027. Based on the performance of MBARS on the ER-2, it will be configured to fly with a fixed antenna pointing near-nadir rather than incorporating the scanning functionality. MBARS is expected to continue to fly on airborne science missions on the NASA Boeing 777 and ER-2 aircraft.

These MBARS flight results also point to the feasibility of global retrievals of atmospheric sea-level pressure from space. Additional flights on NASA aircraft will allow systematic evaluation of retrieval performance at different pointing angles, SNR, and frequency-diversity pulsing configurations. These results could be used to mature the technology readiness of a spaceborne version of MBARS, informing decisions about instrument requirements.

Data availability. MBARS data from the WH^{2}yMSIE field campaign used in the November, 2024 case are available at the NASA/GSFC High Altitude Radar (HAR) website, https://har.gsfc.nasa.gov.

https://doi.org/10.5194/egusphere-2026-1186
Preprint. Discussion started: 9 July 2026

Author contributions. MLWM led the project, performed data analysis and processing, and drafted a version of the manuscript. BL led the development of the retrieval algorithms, processed data, provided figures and drafted sections of the manuscript. NCP assisted in data processing, particularly with respect to data assimilation and MERRA-2 reanalysis data. GMH provided inputs on data processing and algorithm development. LL led the engineering efforts in instrument design and contributed to manuscript text. SH led the development of the flight hardware, the antenna system, and contributed manuscript text and figures. All authors supported data collection and instrument development, and provided feedback on the writing and content.

Competing interests. The authors declare that they have no conflict of interest.

Acknowledgements. This work was funded by the NASA Earth Science Technology Office (ESTO) Instrument Incubator Program (IIP). The WH^{2}yMSIE field campaign was funded by NASA Decadal Survey Incubation (DSI) program and the National Oceanic and Atmospheric Administration (NOAA). The authors would like to thank Gerry McIntire, Eddie Ford, and Michael Coon for their efforts in MBARS development. They would also like to thank the NASA ER-2 pilots and crew, as well as the WH^{2}yMSIE project scientists and the COSMIR-H team for their support during the field campaigns.

https://doi.org/10.5194/egusphere-2026-1186
Preprint. Discussion started: 9 July 2026

References

Barker, D., Huang, W., Guo, Y.-R., and Bourgeois, A.: A three-dimensional variational (3DVAR) data assimilation system for use with MM5, Tech. rep., University Corporation for Atmospheric Research, https://doi.org/doi:10.5065/D6CF9N1J, 2003.

Barker, D. M., Huang, W., Guo, Y.-R., Bourgeois, A. J., and Xiao, Q. N.: A Three-Dimensional Variational Data Assimilation System for MM5: Implementation and Initial Results, Monthly Weather Review, 132, 897 – 914, https://doi.org/10.1175/1520-0493(2004)132<0897:ATVDAS>2.0.CO;2, 2004.

Battaglia, A., Rumi, E., Reeves, R., Sikaneta, I., and D'Addio, S.: Surface Air-Pressure Measurements From Space Using Differential Absorption Radar on the Right Wing of the 60 GHz Oxygen Band, Earth and Space Science, 11, https://doi.org/10.1029/2023EA003374, 2024.

Centurioni, L., Horányi, A., Cardinali, C., Charpentier, E., and Lumpkin, R.: A Global Ocean Observing System for Measuring Sea Level Atmospheric Pressure: Effects and Impacts on Numerical Weather Prediction, Bulletin of the American Meteorological Society, 98, 231 – 238, https://doi.org/10.1175/BAMS-D-15-00080.1, 2017.

Contreras, R. F. and Plant, W. J.: Surface effect of rain on microwave backscatter from the ocean: Measurements and modeling, Journal of Geophysical Research: Oceans, 111, https://doi.org/10.1029/2005JC003356, 2006.

Dirren, S., Torn, R. D., and Hakim, G. J.: A Data Assimilation Case Study Using a Limited-Area Ensemble Kalman Filter, Monthly Weather Review, 135, 1455 – 1473, https://doi.org/10.1175/MWR3358.1, 2007.

Donelan, M. A. and Pierson, Jr., W. J.: Radar scattering and equilibrium ranges in wind-generated waves with application to scatterometry, Journal of Geophysical Research: Oceans, 92, 4971–5029, https://doi.org/10.1029/JC092iC05p04971, 1987.

Foti, G., Gommenginger, C., Jales, P., Unwin, M., Shaw, A., Robertson, C., and Roselló, J.: Spaceborne GNSS reflectometry for ocean winds: First results from the UK TechDemoSat-1 mission, Geophysical Research Letters, 42, 5435–5441, https://doi.org/10.1002/2015GL064204, 2015.

Fukao, S., Hamazu, K., and Doviak, R. J.: Radar for meteorological and atmospheric observations, Springer, https://doi.org/10.1007/978-4-431-54334-3, 2014.

Gelaro, R., McCarty, W., Suárez, M. J., Todling, R., Molod, A., Takacs, L., Randles, C. A., Darmenov, A., Bosilovich, M. G., Reichle, R., Wargan, K., Coy, L., Cullather, R., Draper, C., Akella, S., Buchard, V., Conaty, A., da Silva, A. M., Gu, W., Kim, G.-K., Koster, R., Lucchesi, R., Merkova, D., Nielsen, J. E., Partyka, G., Pawson, S., Putman, W., Rienecker, M., Schubert, S. D., Sienkiewicz, M., and Zhao, B.: The Modern-Era Retrospective Analysis for Research and Applications, Version 2 (MERRA-2), Journal of Climate, 30, 5419 – 5454, https://doi.org/10.1175/JCLI-D-16-0758.1, 2017.

Holton, J. R. and Hakim, G. J.: An introduction to dynamic meteorology, vol. 88, Academic Press, https://doi.org/10.1016/C2009-0-63394-8, 2013.

Hossan, A. and Jones, W. L.: Ku- and Ka-Band Ocean Surface Radar Backscatter Model Functions at Low-Incidence Angles Using Full-Swath GPM DPR Data, Remote Sensing, 13, https://doi.org/10.3390/rs13081569, 2021.

Ingleby, B.: Factors Affecting Ship and Buoy Data Quality: A Data Assimilation Perspective, Journal of Atmospheric and Oceanic Technology, 27, 1476 – 1489, https://doi.org/10.1175/2010JTECHA1421.1, 2010.

Ingleby, B. and Isaksen, L.: Drifting buoy pressures: Impact on NWP, Atmospheric Science Letters, 19, https://doi.org/10.1002/asl.822, 2018.

https://doi.org/10.5194/egusphere-2026-1186
Preprint. Discussion started: 9 July 2026

Karaev, V. Y., Panfilova, M. A., Titchenko, Y. A., Meshkov, E. M., Balandina, G. N., Kuznetsov, Y. V., and Shlaferov, A. L.: Russian scatterometer: discussion of the concept and the numerical simulation of wind field retrieval, International Journal of Remote Sensing, 36, 6056–6084, https://doi.org/10.1080/01431161.2015.1110637, 2015.

Kent, E. C. and Berry, D. I.: Quantifying random measurement errors in Voluntary Observing Ships' meteorological observations, International Journal of Climatology, 25, 843–856, https://doi.org/10.1002/joc.1167, 2005.

Lawrence, R., Lin, B., Harrah, S., Hu, Y., Hunt, P., and Lipp, C.: Initial flight test results of differential absorption barometric radar for remote sensing of sea surface air pressure, Journal of Quantitative Spectroscopy and Radiative Transfer, 112, 247–253, https://doi.org/10.1016/j.jqsrt.2010.06.001, international Symposium on Atmospheric Light Scattering and Remote Sensing (ISALSaRS'09), 2011.

Lawrence, R., Lin, B., Harrah, S., and Min, Q.: Differential Absorption Microwave Radar Measurements for Remote Sensing of Barometric Pressure, in: Remote Sensing - Advanced Techniques and Platforms, edited by Escalante-Ramirez, B., chap. 8, IntechOpen, London, https://doi.org/10.5772/37925, 2012.

Li, L., Heymsfield, G. M., Tian, L., and Racette, P. E.: Measurements of Ocean Surface Backscattering Using an Airborne 94-GHz Cloud Radar—Implication for Calibration of Airborne and Spaceborne W-Band Radars, Journal of Atmospheric and Oceanic Technology, 22, 1033 – 1045, https://doi.org/10.1175/JTECH1722.1, 2005.

Liebe, H. J., Hufford, G. A., and Cotton, M. G.: Propagation modeling of moist air and suspended water/ice particles at frequencies below 1000 GHz, in: Proc. NATO/AGARD Wave Propagation Panel, Malorca, Spain, 1993.

Lin, B. and Hu, Y.: Numerical simulations of radar surface air pressure measurements at O/sub 2/ bands, IEEE Geoscience and Remote Sensing Letters, 2, 324–328, https://doi.org/10.1109/LGRS.2005.848515, 2005.

Lin, B. and Rossow, W. B.: Precipitation water path and rainfall rate estimates over oceans using special sensor microwave imager and International Satellite Cloud Climatology Project data, Journal of Geophysical Research: Atmospheres, 102, 9359–9374, https://doi.org/10.1029/96JD03987, 1997.

Lin, B., Katzberg, S. J., Garrison, J. L., and Wielicki, B. A.: Relationship between GPS signals reflected from sea surfaces and surface winds: Modeling results and comparisons with aircraft measurements, Journal of Geophysical Research: Oceans, 104, 20 713–20 727, https://doi.org/10.1029/1999JC900176, 1999.

Lin, B., Min, Q., and Hu, Y.: Assessing surface air pressure sensing using 118 GHz O2-absorption radar system, Journal of Quantitative Spectroscopy and Radiative Transfer, 261, 107 425, https://doi.org/https://doi.org/10.1016/j.jqsrt.2020.107425, 2021.

Lin, B., Walker Mclinden, M., Heymsfield, G. M., Hu, Y., Privé, N., Li, L., Harrah, S., Horgan, K., Cai, X., and Carswell, J.: Simulations of sea surface reflection for V-band O2 differential absorption radar barometry, Frontiers in Remote Sensing, Volume 4 - 2023, https://doi.org/10.3389/frsen.2023.1105627, 2023.

Lin, B., Walker McLinden, M., Cai, X., Heymsfield, G. M., Privé, N., Harrah, S., and Li, L.: Sea surface barometry with an O2 differential absorption radar: retrieval algorithm development and simulation, Frontiers in Remote Sensing, Volume 5 - 2024, https://doi.org/10.3389/frsen.2024.1399839, 2024.

Mass, C. F. and Madaus, L. E.: Surface Pressure Observations from Smartphones: A Potential Revolution for High-Resolution Weather Prediction?, Bulletin of the American Meteorological Society, 95, 1343 – 1349, https://doi.org/10.1175/BAMS-D-13-00188.1, 2014.

Masuko, H., Okamoto, K., Shimada, M., and Niwa, S.: Measurement of microwave backscattering signatures of the ocean surface using X band and Ka band airborne scatterometers, Journal of Geophysical Research: Oceans, 91, 13 065–13 083, https://doi.org/10.1029/JC091iC11p13065, 1986.

https://doi.org/10.5194/egusphere-2026-1186
Preprint. Discussion started: 9 July 2026

Millán, L., Lebsock, M., Livesey, N., and Tanelli, S.: Differential absorption radar techniques: water vapor retrievals, Atmospheric Measurement Techniques, 9, 2633–2646, https://doi.org/10.5194/amt-9-2633-2016, 2016.

Min, Q., Gong, W., Lin, B., and Hu, Y.: Application of surface pressure measurements from O2-band differential absorption radar system in three-dimensional data assimilation on hurricane: Part I – An observing system simulation experiments study, Journal of Quantitative Spectroscopy and Radiative Transfer, 150, 148–165, https://doi.org/10.1016/j.jqsrt.2014.08.027, 2015a.

Min, Q., Gong, W., Lin, B., and Hu, Y.: Application of surface pressure measurements of O2-band differential absorption radar system in three-dimensional data assimilation on hurricane: Part II — A quasi-observational study, Journal of Quantitative Spectroscopy and Radiative Transfer, 150, 166–174, https://doi.org/10.1016/j.jqsrt.2014.08.026, 2015b.

Privé, N. C., McLinden, M., Lin, B., Moradi, I., Sienkiewicz, M., Heymsfield, G. M., and McCarty, W.: Impacts of Marine Surface Pressure Observations from a Spaceborne Differential Absorption Radar Investigated with an Observing System Simulation Experiment, Journal of Atmospheric and Oceanic Technology, 40, 897 – 918, https://doi.org/10.1175/JTECH-D-22-0088.1, 2023.

Privé, N. C., McLinden, M., Lin, B., Heymsfield, G. M., Cai, X., and Harrah, S.: Observing System Simulation Experiments Exploring Potential Spaceborne Deployment Options for a Differential Absorption Radar Measuring Marine Surface Pressures, Earth and Space Science, 11, https://doi.org/10.1029/2024EA003791, 2024.

Radnóti, G., Bauer, P., McNally, A., and Horányi, A.: ECMWF study to quantify the interaction between terrestrial and space-bsed observing systems on numerical weather prediction skill, Tech. rep., European Centre for Medium-Range Weather Forecasts Tech. Memo, https://doi.org/10.21957/yvf1ceq7i, 2012.

Stiles, B. and Yueh, S.: Impact of rain on spaceborne Ku-band wind scatterometer data, IEEE Transactions on Geoscience and Remote Sensing, 40, 1973–1983, https://doi.org/10.1109/TGRS.2002.803846, 2002.

Tanelli, S., Durden, S. L., Im, E., Pak, K. S., Reinke, D. G., Partain, P., Haynes, J. M., and Marchand, R. T.: CloudSat's Cloud Profiling Radar After Two Years in Orbit: Performance, Calibration, and Processing, IEEE Transactions on Geoscience and Remote Sensing, 46, 3560–3573, https://doi.org/10.1109/TGRS.2008.2002030, 2008.

Walker McLinden, M. L., Li, L., Heymsfield, G. M., Coon, M., and Emory, A.: The NASA GSFC 94-GHz Airborne Solid-State Cloud Radar System (CRS), Journal of Atmospheric and Oceanic Technology, 38, 1001 – 1017, https://doi.org/10.1175/JTECH-D-20-0127.1, 2021.

Whitaker, J. S., Compo, G. P., Wei, X., and Hamill, T. M.: Reanalysis without Radiosondes Using Ensemble Data Assimilation, Monthly Weather Review, 132, 1190 – 1200, https://doi.org/10.1175/1520-0493(2004)132<1190:RWRUED>2.0.CO;2, 2004.

Xiao, Q., Zou, X., and Wang, B.: Initialization and Simulation of a Landfalling Hurricane Using a Variational Bogus Data Assimilation Scheme, Monthly Weather Review, 128, 2252 – 2269, https://doi.org/10.1175/1520-0493(2000)128<2252:IASOAL>2.0.CO;2, 2000.

Xiao, Q., Chen, L., and Zhang, X.: Evaluations of BDA Scheme Using the Advanced Research WRF (ARW) Model, Journal of Applied Meteorology and Climatology, 48, 680 – 689, https://doi.org/10.1175/2008JAMC1994.1, 2009.